



Microstructural characterization of the η -Ni₃(Ti, Al) phase in a long-term-aged Ni-based superalloy

X. B. Hu, X. W. Guo, Y. J. Wang, J. S. Hou, X. Z. Qin, L. Z. Zhou, J. F. Liu & X. L. Ma

To cite this article: X. B. Hu, X. W. Guo, Y. J. Wang, J. S. Hou, X. Z. Qin, L. Z. Zhou, J. F. Liu & X. L. Ma (2017): Microstructural characterization of the η -Ni₃(Ti, Al) phase in a long-term-aged Ni-based superalloy, Philosophical Magazine Letters, DOI: [10.1080/09500839.2017.1406193](https://doi.org/10.1080/09500839.2017.1406193)

To link to this article: <https://doi.org/10.1080/09500839.2017.1406193>



Published online: 06 Dec 2017.



Submit your article to this journal [↗](#)



View related articles [↗](#)



View Crossmark data [↗](#)



Microstructural characterization of the η -Ni₃(Ti, Al) phase in a long-term-aged Ni-based superalloy

X. B. Hu^a, X. W. Guo^{a,b}, Y. J. Wang^a, J. S. Hou^c, X. Z. Qin^c, L. Z. Zhou^c, J. F. Liu^a and X. L. Ma^{a,d}

^aShenyang National Laboratory for Materials Science, Institute of Metal Research, Chinese Academy of Sciences, Shenyang, China; ^bSchool of Materials Science and Engineering, University of Science and Technology of China, Hefei, China; ^cSuperalloys Division, Institute of Metal Research, Chinese Academy of Sciences, Shenyang, China; ^dSchool of Materials Science and Engineering, Lanzhou University of Technology, Lanzhou, China

ABSTRACT

Microstructural features of a geometrically closed packed hexagonal η -Ni₃(Ti, Al) phase precipitated in a long-term-aged Ni-based superalloy are characterised using various kinds of transmission electron microscope (TEM) techniques. The defect features in the η grain interior are clearly revealed at the atomic scale. A nano-sized γ' phase is found at the defect regions of the micro-sized η phase. The interior γ' phase keeps a good orientation relationship (OR) of $(1\ 1\ 1)_{\gamma'}/(0\ 0\ 0\ 1)_{\eta}$ and $[1\ \bar{1}\ 0]_{\gamma'}/[2\ \bar{1}\ \bar{1}\ 0]_{\eta}$ with the η -Ni₃(Ti, Al) phase. However, there is no definitive OR between η -Ni₃(Ti, Al) grains and the surrounding matrix. By means of first-principle calculations, we reveal that a symmetrical interfacial feature between γ' and η corresponds to a lower energy state.

ARTICLE HISTORY

Received 27 March 2017
Accepted 10 November 2017

KEYWORDS

Nickel-based superalloys;
long-term ageing;
transmission electron
microscopy; η -Ni₃(Ti, Al)
phase; interfacial features

1. Introduction

Ni-based superalloys are critical engineering materials that are frequently utilised as hot sections of aircraft engines and gas turbines owing to their superior high-temperature mechanical properties, such as high-temperature strength, creep and fatigue resistance, as well as resistance to corrosion and oxidation [1–3]. In order to gain these superior comprehensive properties, commercial superalloys are always significantly alloyed, which usually involves more than 10 elements. Because of the high degree of alloying, the γ and γ' phases may become supersaturated. Under complex stress and chemical environments during service, the superalloy matrix becomes unstable. As a consequence, the microstructural features of superalloys at high temperature greatly deviate from the pristine microstructure at room temperature. Besides the rafting of the γ' phase [4,5], many different types of secondary phases may precipitate in the matrix [6–12]. Microstructural evolution always exerts important influences on the overall mechanical properties [13–17]. Therefore, it is very important to investigate systematically the microstructural features of these secondary phases to gain a better understanding of the structure–property relationship.

In general, there are three classes of secondary phases in superalloys. One important class is the topological closed packed (TCP) phase such as the Laves, σ , μ and P phases [18,19]. These TCP phases are mainly comprised of transition-metal elements. Regarding their detailed precipitation behaviour and fine microstructural characteristics, there are many available reports [20–22]. The second class of precipitation is the interstitial phase including various kinds of carbides and borides, which are formed by the elements C and B and transition-metal elements. Many studies have focused on their precipitation behaviours and the fine defect features [23–27]. The third class is the geometrically close-packed phase including the γ matrix and the ordered γ' , γ'' , δ and η phases. The η phase possesses the hexagonal $D0_{24}$ lattice, which can be described as Ni_3Ti with many other elements such as Al, Nb, Co and Cr [28]. The η phase always exhibits lamellar and/or rod morphology and its excess precipitation can deteriorate the mechanical properties of superalloys. However, the precipitation of η phase can be controlled by the addition of Al, Ti, Co and other elements [29,30]. The η phase precipitated discontinuously along grain boundaries was recently considered to be beneficial in enhancing the mechanical properties of the newly developed polycrystalline turbine disk alloy ALLvac 718Plus [31]. Besides the intergrowth with the δ phase [32], this locally nano-sized η phase also exists in the stacking-fault regions of the matrix [33]. The phase transformation from γ' to nano-sized η phase was recently highlighted as a strengthening manner for wrought superalloys [34]. Through the above phase transformation, the deleterious deformation mode of nano-twinning above 973 K can be effectively inhibited. The reverse transformation of the η phase to face-centred cubic austenite during isothermal ageing was discovered in a Fe–Ni–Ti alloy [35]. Until now, most previous work related to the η phase focused on the turbine disk alloys aged/deformed with a relative short thermal history. In this study, we reveal the different microstructural features of the η phase precipitated in a polycrystalline turbine-blade alloy subjected to a long-term ageing treatment.

2. Experimental procedures and calculation methods

An experimental hot corrosion-resistant polycrystalline Ni-based superalloy was utilised in the present study. Its nominal chemical composition is 15.5Cr, 10.8Co, 2.1Mo, 5.6 W, 3.2Al, 4.6Ti, 0.2Nb, 0.4Hf, 0.073C, 0.075B and balance Ni in weight per cent. The as-cast alloy was solution treated at 1443 K for 4 h, then aged at 1323 K for 4 h and finally aged at 1123 K for 16 h followed by air cooling. After the above standard heat treatment, the samples were subjected to a long-term ageing treatment, exposed at 1173 K for 10,000 h followed by air cooling. An electron-transparent specimen was prepared by the conventional grinding, dimpling and ion-milling method.

Electron diffraction patterns (EDPs) and dark-field (DF) images were acquired using a JEM-2100 operated at 200 kV. The atom-resolution high-angle annular dark field (HAADF) images and chemical composition analyses were obtained using an aberration-corrected Titan³™ G² 60-300 TEM equipped with a high-brightness field-emission gun (X-FEG), a double Cs correctors from CEOS, a monochromator and an X-ray energy-dispersive spectrometer (EDS) system. The operating voltage was set as 300 kV. The convergence semi-angle of the electron beam is approximate 25 mrad for HAADF imaging, yielding a probe size less than 0.10 nm. The collection angle of the HAADF detector ranges from 50 to 250 mrad. The final resolution approximates to 0.08 nm for HAADF imaging.

The calculations presented in this work were based on density functional theory (DFT) as implemented in the VASP code [36]. The GGA-PW91 version [37] of the exchange-correlation energy function was used with the projector augmented wave (PAW) method [38]. The plane-wave cut-off energy was chosen as 500 eV. The optimised lattice parameters of Ni₃Ti and Ni₃Al are $a_{\text{Ni}_3\text{Ti}} = 5.108 \text{ \AA}$, $c_{\text{Ni}_3\text{Ti}} = 8.351$ and $a_{\text{Ni}_3\text{Al}} = 3.569 \text{ \AA}$, which are close to previous calculated and experimental results [39,40].

We considered a series of interface models between γ' -Ni₃Al (1 1 1) and η -Ni₃Ti (0 0 1) and calculated the work to separate them according to the formula: [41]:

$$W_{\text{sep}} = (E_{\text{Ni}_3\text{Ti}} + E_{\text{Ni}_3\text{Al}} - E_{\text{int}})/2A, \quad (1)$$

where E_{int} , $E_{\text{Ni}_3\text{Ti}}$ and $E_{\text{Ni}_3\text{Al}}$ are the total energies of the interface model and the two slab models containing the isolated Ni₃Ti and Ni₃Al parts. A is the interface area, and the factor 2 is introduced since there are two interfaces in the models. For the Monkhorst–Pack [42] k -point mesh, we have tested several cases with k -point meshes of $4 \times 4 \times 1$, $6 \times 6 \times 1$ and $8 \times 8 \times 1$, and found that $6 \times 6 \times 1$ was enough to give reasonable results. In this definition, a larger value of the work to separate corresponds to a more stable interface model. The ionic relaxation was considered as convergent when the force on every atom was less than 10 meV/Å.

3. Results and discussion

Figure 1a is a DF image that shows the blocky η phase precipitated in the long-term-aged samples. Obviously, many long planar defects exist in the interior of the η grain as indicated by the arrows. Figures 1b and 1c are selected-area electron diffraction (SAED) patterns that were obtained from the defect-free regions via continuously tilting along the [0 0 0 1] direction and indexed as $[2 \bar{1} \bar{1} 0]$ and $[1 0 \bar{1} 0]$ zone axes, respectively. Based on the electron diffraction patterns (EDPs), the lattice parameters of the η phase can be derived as $a = 0.51 \text{ nm}$, $c = 0.83 \text{ nm}$ with the space group $P6_3/\text{mmc}$. Owing to the intrinsic microcosmic symmetry of the η phase, structural extinction [?] always happens. Because the c glide plane is perpendicular to the $\langle 1 \bar{1} 0 0 \rangle$ crystallographic direction, $\{hh \bar{2}h l\}$ reflections disappear, where l is odd as shown in Figure 1c. On account of the 6_3 screw axis along the [0 0 0 1] direction, $\{0 0 0 l\}$ reflections should vanish when l is odd in EDPs as illustrated in Figure 1c. However, along the $[2 \bar{1} \bar{1} 0]$ zone axis shown in Figure 1b, all reflections appear because of dynamic diffraction. Large-angle tilting experiments shows that there are no definitive rational ORs between the η phase and the neighbouring matrix. As shown in EDPs of Figure 1d, the matrix deviates from the $[1 1 \bar{2}]_{\text{M}}$ zone axis by $\sim 6^\circ$ when the η phase is exactly in the $[2 \bar{1} \bar{1} 0]$ direction. In addition, as demonstrated in the composite EDPs shown in Figure 1e, there are no rational planes in the η phase that correspond to the planes in the matrix. To gain chemical information for these inhomogeneous regions in the η phase, we utilise the EDS mapping technique implemented in the scanning TEM mode. Figure 2a shows the real-time HAADF image, in which the matrix and η phases are indicated. Figures 2b–d show the element maps imaged by Ni-K, Al-K and Ti-K, respectively. Compared with the perfect region, these defect regions (indicated in the DF image in Figure 1a) are richer in Al but poorer in Ti, while the content of Ni is similar. Therefore, the long dark contrasts in Figure 2a probably correspond to the γ' phase, which is much richer in Al.

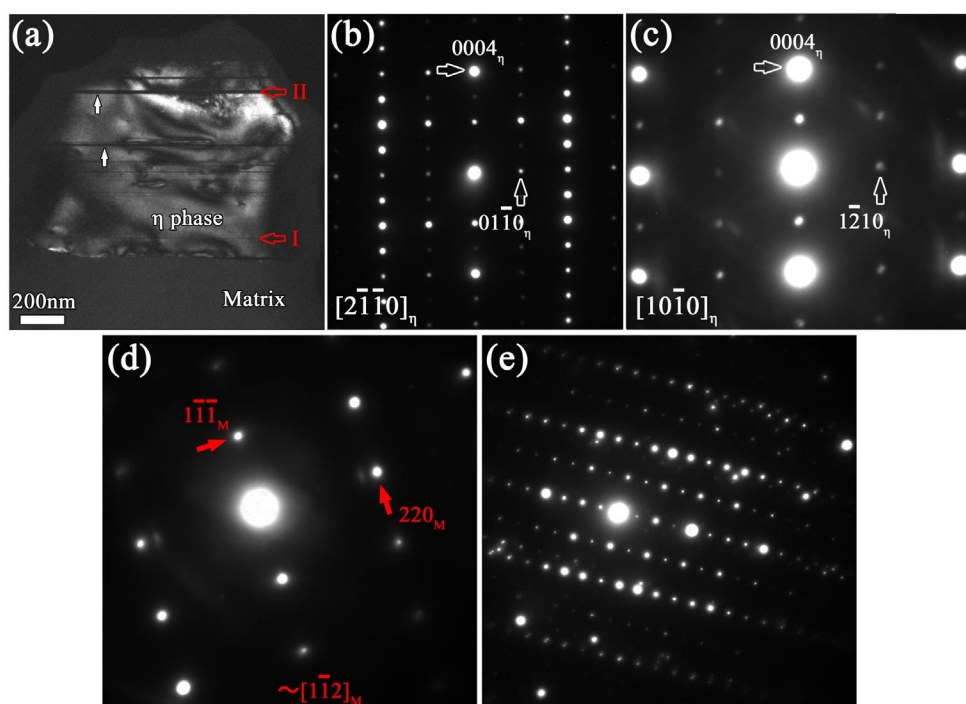


Figure 1. (a) Dark-field (DF) image showing the η phase precipitated in the γ/γ' matrix in the long-term-aged sample. The DF image is generated using the $(0\ 0\ 0\ 4)_{\eta}$ reflection. Arrows indicated the defect regions in the grain interior. Horizontal arrows indicated two regions used for atomic resolution imaging analyses. (b) and (c) Electron diffracting patterns (EDPs) recorded from the perfect region inside η . (d) The corresponding EDPs obtained from the matrix when the η phase is in the exact $[2\bar{1}\bar{1}0]_{\eta}$ direction. (e) The composite EDPs obtained from the regions including both matrix and η phase.

In order to visualise more details for these defects, structural features were revealed at a higher spatial resolution. Figure 3a shows the composite EDPs recorded from both the perfect and the defect areas in the η phase. Based on careful analyses, this composite EDPs can be indexed as the η phase and twinned γ' as shown by the frames indicated in Figure 3a. Furthermore, this nano-sized γ' phase maintains a good crystallographic OR with the surrounding η phase, which can be best described as $(1\ 1\ 1)_{\gamma'}/(0\ 0\ 0\ 1)_{\eta}$ and $[1\bar{1}\bar{1}0]_{\gamma'}/[2\bar{1}\bar{1}0]_{\eta}$. The atomic-resolution HAADF image in Figure 3b shows the fine microstructural features of γ' sandwiched by η phases. It is seen that the localised structural fragments within the γ' and η phases neighbouring the interfaces are symmetrical (as indicated) for both top and bottom interfaces. The microstructural features that a single unit cell of the η phase sandwiched by γ' phases were also studied. Although possessing different configurations from Figure 3b, these localised stacking layers within the γ' and η phases near the interface are also symmetrical. As discussed in our previous work [43], the formation of γ' phases in the interior of a $M_{23}C_6$ grain is closely related to that of supersaturated Ni and Al elements in $M_{23}C_6$ carbide. Thus, the formation of nano-sized γ' phases in the interior of a η grain is probably related to a redistribution of elements in the η phase, which helps to relieve the supersaturated Al. However, differing from the micro-sized η phase, which shows no definitive ORs with the surrounding matrix, the precipitated nano-sized γ' phase retains a

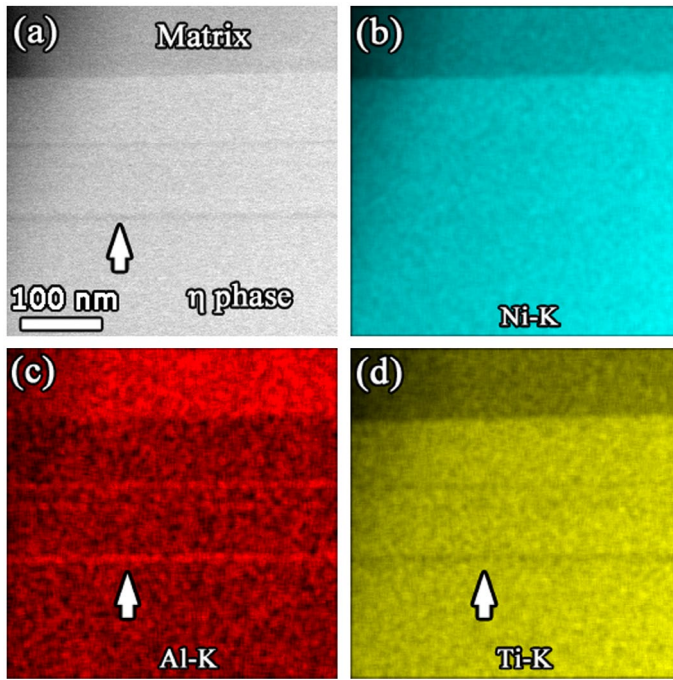


Figure 2. (a) High-magnification HAADF image showing the long dark contrasts (indicated by the arrow) in the η phase. (b)–(d) Element map imaged by Ni-K, Al-K and Ti-K, respectively showing relative element distributions.

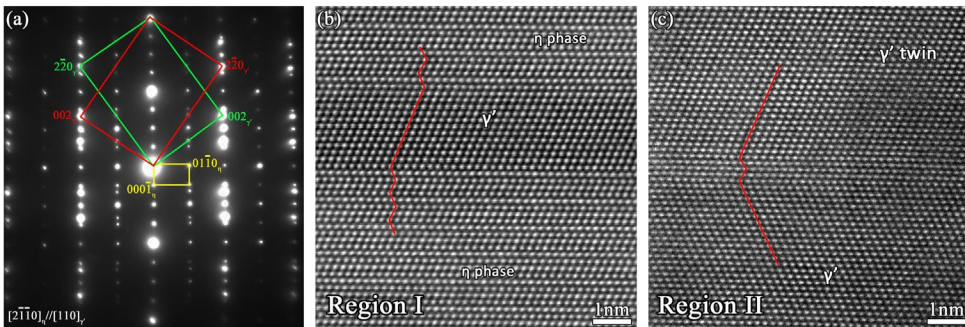


Figure 3. (a) Composite EDPs recorded from the η grain interior including defect regions. (b), (c) Atomic-resolution HAADF images obtained from regions I and II, respectively (indicated in Figure 1a) showing the fine structural features of the planar defect within the η phase.

very good OR with the surrounding η phase. This may result from the lattice strain between η and γ' [35]. Because of the strain energy, the ORs are good when the grain size is small, but if the grain size becomes large the ORs will be destroyed.

In order to further understand these interfacial features, and hence clarify the phase transformation from the γ' to the η phase [34], we performed first-principles calculations. Figure 4a and b show the atomic stacking sequences of the γ' -Ni₃Al and η -Ni₃Ti phases, respectively. It is obvious that these can be described as AC'B'AC'B'A' and ABACABA,

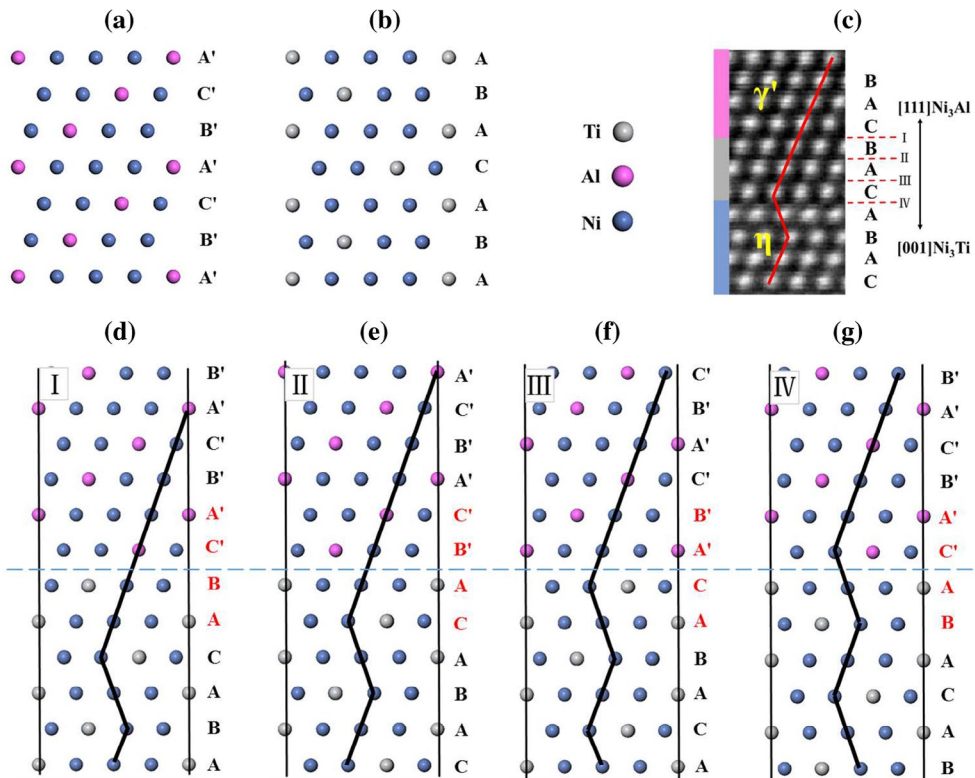


Figure 4. Atomic models of the interface between γ' -Ni₃Al and η -Ni₃Ti. (a) and (b) atomic stacking of γ' -Ni₃Al along the [1 1 1] direction and of η -Ni₃Ti along the [0 0 1] direction, respectively. (c) Experimental image and the stacking sequence of the interface. (d–g) four possible interface models I–IV with the interfaces indicated by dashed lines. The red solid line in (c) and the black solid lines in (d–g) highlight the interfacial stacking sequences.

Table 1. The interface separation work (in J m⁻²) of the four different interfacial models between Ni₃Al and Ni₃Ti.

Interface	I	II	III	IV
W_{sep}	4.03	4.01	3.84	3.85

respectively. From the zoomed-in experimental image of the interface showed in Figure 4c, the stacking sequence of the interface can be described as ...BAC-[BAC]-ABAC.... The BAC in the bracket can be considered as the stacking sequence of either γ' -Ni₃Al or η -Ni₃Ti. Based on the experimentally determined atomic stacking sequence, four possible interfacial models were constructed and labelled I, II, III and IV as shown in Figure 4d–g, respectively.

From the calculated results listed in Table 1, we can see that the interface separation work of model II is very close to that of model I (a difference of about 0.02 J/m²) and the difference between models III and IV is also very close (about 0.01 J/m²), while the averaged separation work of models I and II is 0.17 J/m² larger than that of models III and IV. Thus, the four models can be classified into two groups: (I, II) and (III, IV), and both models I and II in the first group are the more likely interfacial configurations. Based on this result, we have successfully reduced the uncertainty of the interface section from three layers, i.e.

the BAC layers, into one layer, namely the B layer. In this layer, either Al or Ti could exist, resulting in similar values of the interface separation work.

To reveal the intrinsic structural characteristics, the atomic stacking sequences near the interfaces were further analysed as shown in Figure 4d–g. The stacking sequence around the interface in model I is ACBA, which changes into CBAC (model II) when a horizontal displacement is applied. Both stacking sequences could be regarded as being of the γ' type. The atomic stacking sequences around the interfaces in models III and IV are also closely related. The sequence ACAB in model III will change into BACA in model IV when an operation of mirror symmetry is applied, if the difference between Al and Ti is neglected. Both stacking sequences could be regarded as η type. That is the reason why the interface separation work of models I and II are very close as are those of models III and IV. If the atomic layers around interfaces adopt the stacking sequence of γ' type, the interface will be more stable.

4. Conclusions

From the systematic microstructural investigations of the η -Ni₃(Ti, Al) phase precipitated in a long-term-aged Ni-based superalloy reported here, the following conclusions can be drawn. The η -Ni₃(Ti, Al) phase has no definitive OR with the surrounding matrix. The defect region in the interior of the η grain was determined to be the nano-scaled γ' phase, which keeps a good OR with the surrounding η phase; this can be described as $(1\ 1\ 1)\gamma'//[0\ 0\ 0]_{\eta}$ and $[1\ \bar{1}\ 0]_{\gamma'}//[2\ \bar{1}\ 0]_{\eta}$. Atomic-resolution HAADF images reveal that the localised stacking layer within the γ' phase and the η phases neighbouring the interfacial regions are symmetrical with the stacking sequence BAC-[BAC]-ABAC. BAC indicates the interfacial stacking layers and can represent either γ' -Ni₃Al or η -Ni₃Ti. From first-principles calculations, the observed symmetrical interfacial feature possesses a lower interfacial energy. In addition, the uncertainty of the interface model is reduced from BAC layers into a B layer.

Acknowledgements

We are grateful to Mr J. Wang for bulk sample preparation, and to Mr B. Wu and Mr L.X. Yang for technical support on the Titan platform.

Disclosure statement

No potential conflict of interest was reported by the authors.

Funding

This work was supported by the National Natural Science Foundation of China [grant number 11327901], [grant number 51390473] and [grant number 51571191].

References

- [1] R.C. Reed, *The Superalloys: Fundamentals and Applications*, Cambridge University Press, Cambridge, 2006.
- [2] T.M. Pollock and S. Tin, *J. Propul. Power.* 22 (2006) p.361–374.

- [3] J.H. Perepezko, *Science*. 326 (2009) p.1068–1069.
- [4] M. Kamaraj, C. Mayr, M. Kolbe and G. Eggeler, *Scripta Mater.* 38 (1998) p.589–594.
- [5] R.C. Reed, N. Matan, D.C. Cox, M.A. Rist and C.M.F. Rae, *Acta Mater.* 47 (1999) p.3367–3381.
- [6] X.B. Hu, Y.L. Zhu, L.Z. Zhou, B. Wu and X.L. Ma, *Philos. Mag. Lett.* 95 (2015) p.237–244.
- [7] X.B. Hu, L.Z. Zhou, J.S. Hou, X.Z. Qin and X.L. Ma, *Philos. Mag. Lett.* 96 (2016) p.273–279.
- [8] X.Z. Qin, J.T. Guo, C. Yuan, J.S. Hou, L.Z. Zhou and H.Q. Ye, *Mater. Sci. Eng. A* 543 (2012) p.121–128.
- [9] M.J. Kaufman and V.I. Levit, *Philos. Mag. Lett.* 88 (2008) p.259–267.
- [10] B. Du, Z. Shi, J. Yang, Z. Chu, C. Cui, X. Sun, L. Sheng and Y. Zheng, *J. Mater. Sci. Technol.* 32 (2016) p.265–270.
- [11] G. Lvov, V. Levit and M. Kaufman, *Metall. Mater. Trans. A* 35 (2004) p.1669–1679.
- [12] X.B. Hu, Y.B. Xue, S.J. Zheng, Y.L. Zhu, D. Chen and X.L. Ma, *J. Alloy. Compd.* 611 (2014) p.104–110.
- [13] W. Mo, S. Lu, D. Li and Y. Li, *Metall. Mater. Trans. A* 45 (2014) p.5114–5126.
- [14] J. Wang, L.Z. Zhou, X.Z. Qin, L.S. Sheng, J.S. Hou and J.T. Guo, *Mater. Sci. Eng. A* 553 (2012) p.14–21.
- [15] L.R. Liu, T. Jin, N.R. Zhao, Z.H. Wang, X.F. Sun, H.R. Guan and Z.Q. Hu, *Mater. Sci. Eng. A* 385 (2004) p.105–112.
- [16] L. Xiao, D.L. Chen and M.C. Chaturvedi, *Metall. Mater. Trans. A* 35 (2004) p.3477–3487.
- [17] J.Y. Chen, Q. Feng and Z.Q. Sun, *Scripta Mater.* 63 (2010) p.795–798.
- [18] K.H. Kuo, *J. Mater. Sci.* 21 (1986) p.2597–2622.
- [19] F. Sun and J.X. Zhang, *Adv. Mater. Res.* 320 (2011) p.26–32.
- [20] D.S. Zhou, H.Q. Ye and K.H. Kuo, *Philos. Mag. A* 57 (1988) p.907–922.
- [21] H.Q. Ye, D.N. Wang and K.H. Kuo, *Philos. Mag. A* 51 (1985) p.839–848.
- [22] C.M.F. Rae and R.C. Reed, *Acta Mater.* 49 (2001) p.4113–4125.
- [23] H.R. Zhang and O.A. Ojo, *Philos. Mag.* 90 (2010) p.765–782.
- [24] X.B. Hu, Y.L. Zhu and X.L. Ma, *Acta Mater.* 68 (2014) p.70–81.
- [25] X.B. Hu, Y.L. Zhu, X.H. Shao, H.Y. Niu, L.Z. Zhou and X.L. Ma, *Acta Mater.* 100 (2015) p.64–72.
- [26] X.B. Hu, Y.L. Zhu, N.C. Sheng and X.L. Ma, *Sci. Rep.* 4 (2014) p.7367.
- [27] N. Sheng, X. Hu, J. Liu, T. Jin, X. Sun and Z. Hu, *Metall. Mater. Trans. A* 46 (2015) p.1670–1677.
- [28] S. Antonov, M. Detrois, R.C. Helmink and S. Tin, *J. Alloy. Compd.* 626 (2015) p.76–86.
- [29] L. Xu, C. Cui and X. Sun, *Mater. Sci. Eng. A* 528 (2011) p.7851–7856.
- [30] C.Y. Cui, Y.F. Gu, D.H. Ping, T. Fukuda and H. Harada, *Mater. Trans.* 49 (2008) p.424–427.
- [31] E.J. Pickering, H. Mathur, A. Bhowmik, O.M.D.M. Messé, J.S. Barnard, M.C. Hardy, R. Krakow, K. Loehnert, H.J. Stone and C.M.F. Rae, *Acta Mater.* 60 (2012) p.2757–2769.
- [32] O.M. Messé, J.S. Barnard, E.J. Pickering, P.A. Midgley and C.M.F. Rae, *Philos. Mag.* 94 (2014) p.1132–1152.
- [33] T.M. Smith, B.D. Esser, N. Antolin, G.B. Viswanathan, T. Hanlon, A. Wessman, D. Mourer, W. Windl, D.W. McComb and M.J. Mills, *Acta Mater.* 100 (2015) p.19–31.
- [34] T.M. Smith, B.D. Esser, N. Antolin, A. Carlsson, R.E. Williams, A. Wessman, T. Hanlon, H.L. Fraser, W. Windl, D.W. McComb and M.J. Mills, *Nat. Commun.* 7 (2016) p.13434.
- [35] Y.-U. Heo, M. Takeguchi, K. Furuya and H.-C. Lee, *Acta Mater.* 57 (2009) p.1176–1187.
- [36] G. Kresse and J. Furthmüller, *Phys. Rev. B* 54 (1996) p.11169–11186.
- [37] J.P. Perdew, J.A. Chevary, S.H. Vosko, K.A. Jackson, M.R. Pederson, D.J. Singh and C. Fiolhais, *Phys. Rev. B* 46 (1992) p.6671–6687.
- [38] G. Kresse and D. Joubert, *Phys. Rev. B* 59 (1999) p.1758–1775.
- [39] P.V.M. Rao, K.S. Murthy, S.V. Suryanarayana and S.V.N. Naidu, *Phys. Status Solidi A* 133 (1992) p.231–235.
- [40] J.L. Glimois, P. Forey, R. Guillen and J.L. Feron, *J. Less-Common Met.* 134 (1987) p.221–228.
- [41] H.J. Monkhorst and J.D. Pack, *Phys. Rev. B* 13 (1976) p.5188–5192.
- [42] I.I. Oleinik, E.Y. Tsybmal and D.G. Pettifor, *Phys. Rev. B* 65 (2001) p.020401.
- [43] X.B. Hu, X.Z. Qin, J.S. Hou, L.Z. Zhou and X.L. Ma, *Philos. Mag. Lett.* 97 (2017) p.43–49.